FR-60436

A Final Report for:

SUPERHARD NANOCRYSTALLINE HOMOMETALLIC STAINLESS STEEL ON STEEL FOR SEAMLESS COATINGS

Contract Period

2 November 2001 through 1 November 2002

Submitted under:

Contract No. NAS1 02041

Submitted to:

Office of Procurement
Attn: Bessie Nicholson, Mail Stop 126
NASA Langley Research
Mark for NAS1 02041
Hampton, VA 23681-2199

Prepared by:

Eric Tobin

Submitted by:

Spire Corporation
One Patriots Park
Bedford, MA 01730-2396

PROJECT SUMMARY

The overall objective of this work is to develop a technology for deposition of nanocrystalline, homometallic (an integrated layer without interface), superhard, adherent, scratch and corrosion-resistant coatings for protection of materials used in aerospeace applications. Homometallic coatings are coatings that have almost equivalent composition to the metallic substrates of devices onto which they are deposited. However, their nanocrystalline structures provide enhancement in important properties such as increased hardness, toughness and wear and corrosion resistance, without the brittleness, poor adhesion and other problems associated with conventional ceramic coatings.

Homometallic coatings have tremendous potential to improve the properties of a variety of components. In Phase I we have deposited nanocrystalline, homometallic 316L stainless steel coatings by ion beam assisted deposition (IBAD), a low temperature, high vacuum process that combines evaporation with concurrent ion bombardment. The ions and the current density of the ion beam were varied to produce a variety of different coatings. Substrates included 316L stainless steel coupons, Si wafers, and 0.005" thick spring steel stress coupons. Processing variations were limited to ion beam current density during coating and composition of the ion beam; initial coating runs were conducted with mixtures of Ar^+ and N_2^+ ions for a comparison with Ar^+ ions alone.

For all deposition conditions we achieved smooth, uniform, superhard coatings. All coatings were at least 200 percent harder than the bulk materials, with samples produced at higher current density up to 400 percent harder. The best sample showed about a 30 times lower wear rate than the uncoated material.

Although Phase I results for nanocrystalline stainless steel coatings were extremely successful, Phase II work will concentrate on nanocrystalline, homometallic coating of Ti alloys. This decision was made based on our discussion with Dr. Robert Hafley, the Phase I's technical monitor, and other NASA scientists. Reducing corrosion and wear of Ti alloys would have a more significant impact on aerospace and NASA applications.

TABLE OF CONTENTS

1 BACKGROUND

1.1 Overview

The overall objective of this work is to develop a technology for deposition of nanocrystalline, homometallic (an integrated layer without interface-see Figure 1), superhard (see Figures 2 and 3), adherent, scratch and corrosion-resistant (see Figure 4) coatings for protection of materials used in aerospace applications. Homometallic coatings are coatings that have almost equivalent composition to the metallic substrates or devices onto which they are deposited. However, their nanocrystalline structures provide enhancement in important properties such as increased hardness, toughness and wear and corrosion resistance, without the brittleness, poor adhesion and other problems associated with conventional ceramic coatings.

Homometallic coatings have tremendous potential to improve the properties of a variety of components. In Phase I we have deposited nanocrystalline, homometallic 316L stainless steel coatings by ion beam assisted deposition (IBAD), a low temperature, high vacuum process that combines evaporation with concurrent ion bombardment. The ions and the current density of the ion beam were varied to produce a variety of different coatings. For all deposition conditions we achieved smooth, uniform, superhard coatings. All coatings were at least 200 percent harder than the bulk materials, with samples produced at higher current density up to 400 percent harder. The best sample showed about a 30 times lower wear rate than the uncoated material.

Although Phase I results for nanocrystalline stainless steel coatings were extremely successful, Phase II work will concentrate on nanocrystalline, homometallic coating of Ti alloys. This decision was made based on our discussion with Dr. Robert Hafley, the Phase I's technical monitor, and other NASA scientists. Reducing corrosion and wear of Ti alloys would have a more significant impact on aerospace and NASA applications.

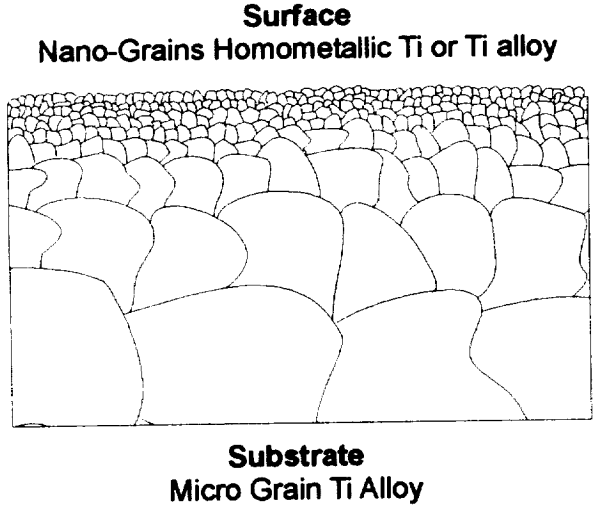

Figure 1 Schematic of a graded nanocrystalline homometallic Ti or Ti alloy coating deposited on a microcrystalline Ti substrate for enhancing hardness, wear and scratch resistance. The coating would have essentially the same composition and phase as the substrate and would consist of much smaller (100 to 400 times) grains.

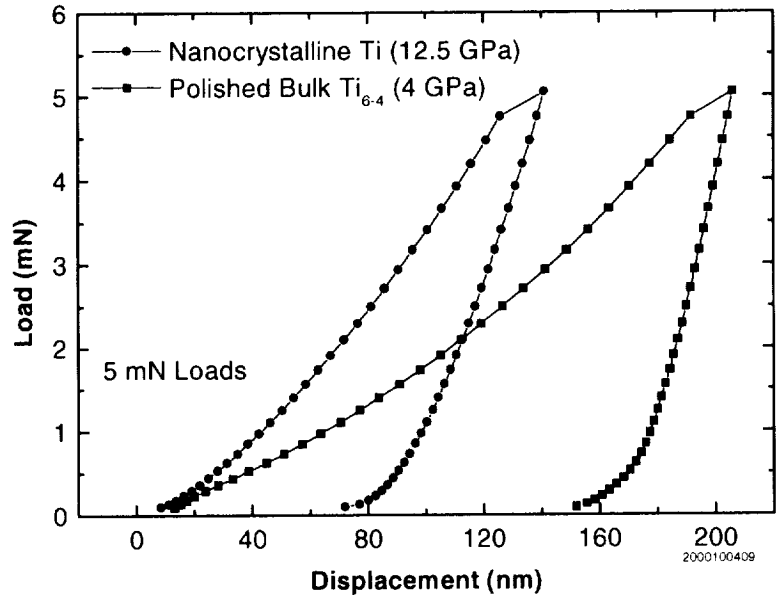

Figure 2 **Comparison of nanoindentation loading and unloading curves for nanocrystalline Ti-6Al-4V film and bulk (large grains) Ti-6Al-4V for a load of 5mN. As can be seen, the depth of indenter penetration is lower for the nanocrystalline films, giving rise to a higher hardness. In addition, for the bulk (large grained) Ti-6Al-4V, the plastic deformation is significant (170 nm) with most of the indenter displacement accommodated plastically and only a small portion being recovered on unloading. On the other hand, for the nanocrystalline, film plastic deformation is much smaller (85 nm).**

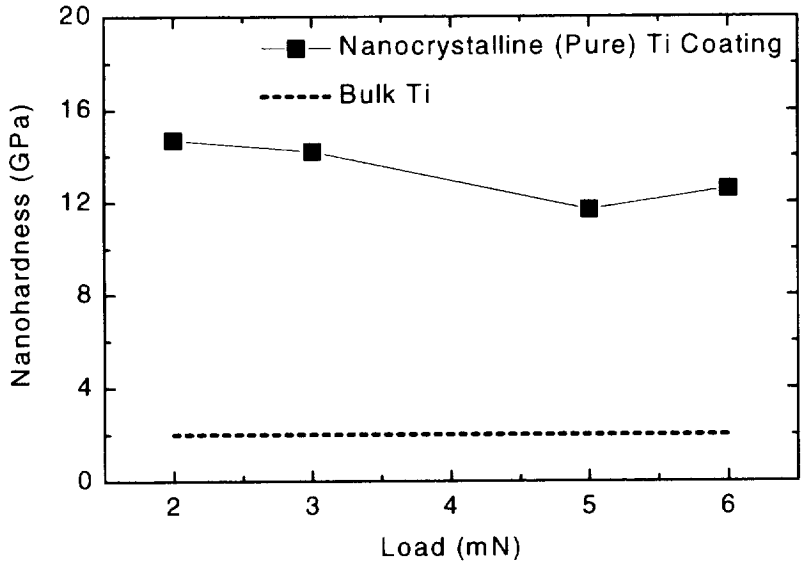

Figure 3 **Comparison of nanoindentation for bulk Ti-6Al-4V with nanocrystalline (<40 nm grains) homometallic Ti-6Al-4V coatings. The increased hardness is due to reduction of grain size.**

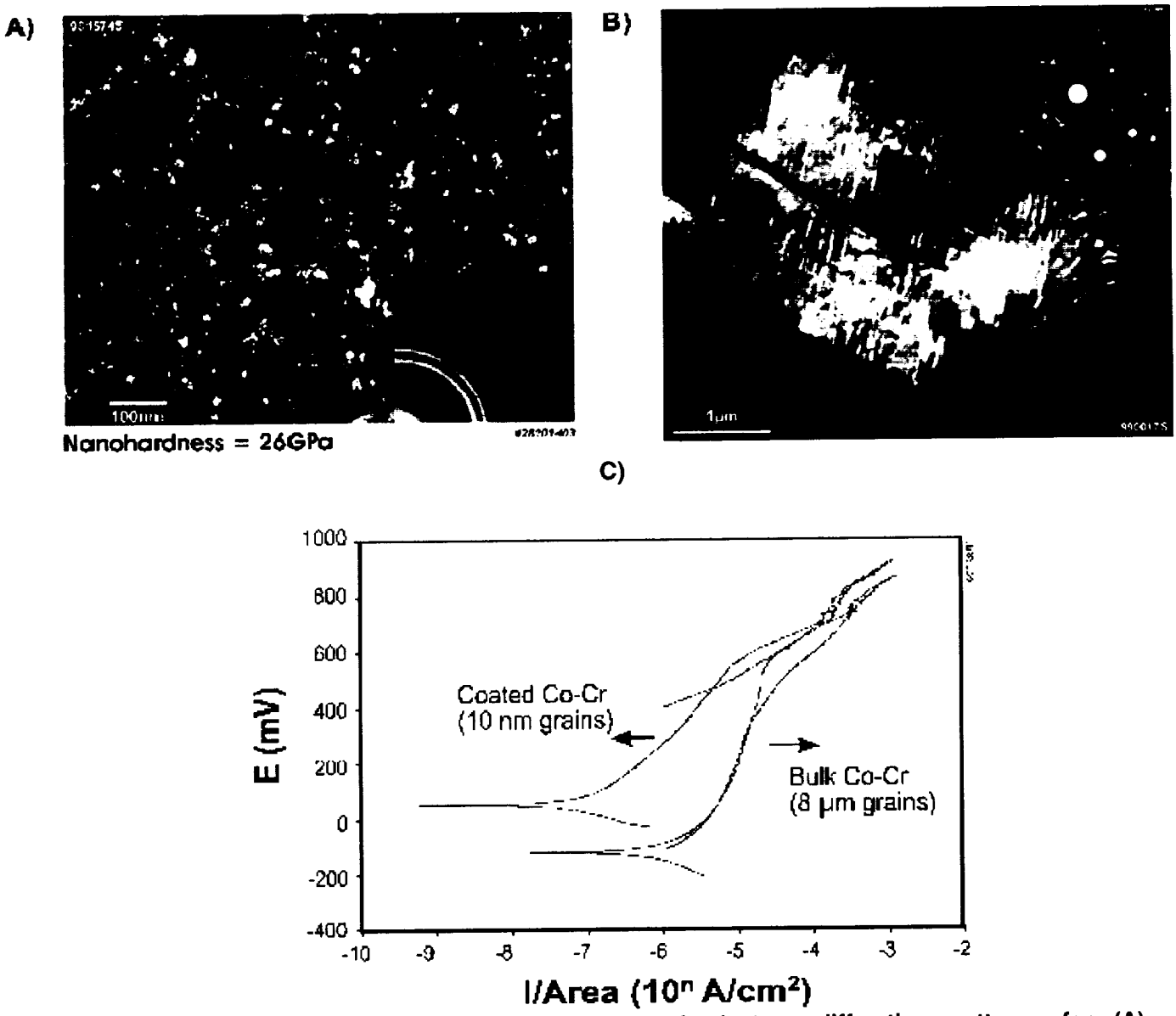

Figure 4 (A and B) Dark-field TEM images and electron diffraction patterns for (A) nanocrystalline Co-Cr coating with a hardness of 26 GPa and (B) ASTM F799 Co-Cr-Mo substrate with a hardness of 6 GPa. (C) Potentiodynamic polarization curve for the nanocrystalline homometallic coating shows ~1.5 decades displacement from the bulk Co-Cr-Mo, indicating at least an order of magnitude decreased corrosion rate.

1.2 Application of Nanocrystallites to Reduce Wear and Corrosion

Empirical processes for producing steel with exceptional combinations of hardness and toughness have long been established, although not understood. The most famous example of this is "Damascus steel," recognized as having exceptional properties from as early as 300 B.C. through the time of the Crusades. Even today the method used to produce these materials is not clearly understood. Metallurgical investigation has shown that these materials have micron-sized crystallites.

1.2.1 Protective coatings

Although much progress has been made in material processing techniques and in the development of new alloys, performance is still inadequate for some demanding applications. In many applications higher performance is desired, yet short-term development of new bulk materials or further improvements in existing alloys seems unlikely (or at least very expensive). In such cases, protective coatings can significantly improve performance. Coatings have become extremely important in applications where corrosion and wear resistance and low-friction are required, and there is great potential for advanced coating technologies to push forward the limit of performance of many current materials. Loss of productivity and material due to friction and wear accounts for a few percent of the GNP of developed countries – in the hundreds of billions of dollars a year for the U.S. alone.[1]

1.2.2 Relevant Issues and Problems Associated with Protective Hard Coatings

An operational and reliable protective coating requires good adhesion and high wear resistance. Good adhesion is dependent upon good chemical bonding between the coating and substrate, as well as good interfacial contact. By virtue of using ion-enhanced deposition in this program, problems with interfacial contact are minimized. However, even using ion assistance, adhesive failure can still result from high residual stress in a ceramic film due to differences in thermal and compositional properties of the coating and substrate.

The protection of surfaces by hard coatings has potential to become one of the most important and versatile means of improving their performance. There are, however, important and, to date difficult, issues involved in the production of reliable coatings. Problems with coatings arise primarily because many desired properties of the substrate-coating interface, such as good adherence to the substrate, lack of surface interactions, and/or high hardness and high toughness of the layer, cannot be obtained simultaneously in known (conventional/ceramics) coating materials. As the hardness and strength increase, toughness and adherence to the substrate decrease.

The chemical bonding characteristics of hard materials has a strong influence on their adherence to substrates as well as their adhesion to other materials. In general, materials for hard coatings[2] possess three primary types of bonding configurations: metallic, covalent, and ionic (see Figure 5). Those with metallic bonding are tough and ductile. Covalently bonded materials are hard and strong, and generally possess high wear resistance. Examples include diamond, diamond-like carbon, SiC, carbon nitride, and cubic boron nitride. Ionic materials, such as alumina and zirconia, are typically hard, stable, and inert. Most ceramics possess a combination of bonding types; however, ionic and covalent bonds typically dominate (tungsten carbide exhibits one of the highest metallic bonding behaviors of any ceramic). It is this fundamental difference in chemical bonding that leads to problems when attempting to deposit ceramic coatings such as BN, AlN, SiC and B_4C on metallic materials. Intermediate layers are used to increase adhesion (*e.g.* Ti, Cr, Ni), but bonding is still often inadequate.

1.2.3 Why Nanocrystallites Enhance the Properties of Protective Coatings

Films comprised of nanocrystalline materials often have mechanical properties that differ from those of materials having larger grains. One fundamental reason for this is that, for grain sizes smaller than 100 nm, the volume of material influenced by proximity to a grain boundary becomes significant. At a grain size of about 5 nm, approximately 50% of the volume is "near grain boundary" material. Such structural changes have a strong influence on the most fundamental of material properties such as elastic modulus (E) and conductivity.

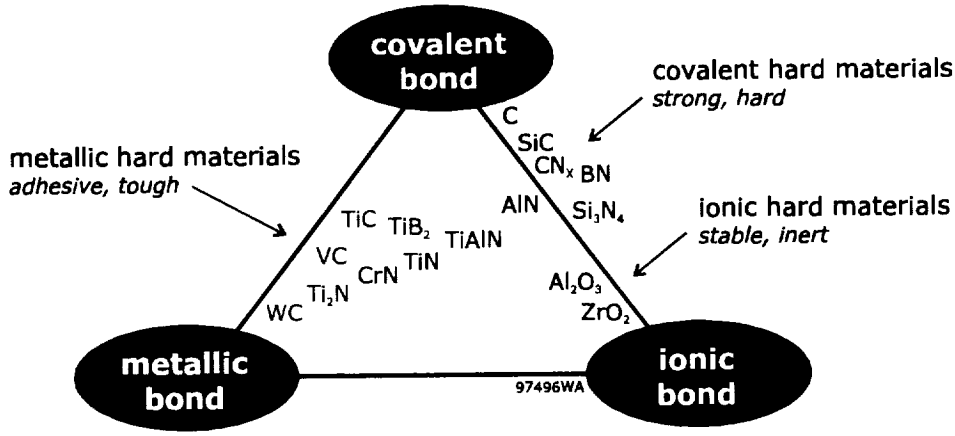

Figure 5 Relative bonding configurations of typical hard coating materials. Adhesion problems typically encountered when applying ceramic coatings to metallic substrates are due to the strong covalent/ionic bonding nature of ceramics (the reason for their hardness), which is incompatible with the metallic bonding characteristic of metals.

1.2.4 Metallic (Ductile) Materials

The strategy on which the development of hard nanocrystalline materials is based depends partly on the material used. More important is the failure mode being avoided. For ductile materials such as metals the failure mode is deformation facilitated by dislocation motion. The benefit of small grains for increased hardness (known as the Hall-Petch[3,4] relation, $H \sim d^{-1/2}$) is twofold (see Figure 6). The boundaries between small grains are barriers to dislocation motion against which only a small number of dislocations can pile up, because the grain dimension is too small for many dislocations to form. The fine grain structure essentially "spreads out" the stress of dislocation pileups between many small grains as opposed to fewer (but larger and higher-stress) pileups at the boundaries between large grains. The second reason nanocrystalline ductile materials resist deformation is that the small dimension inhibits the primary mechanisms for dislocation generation, such as the Frank-Reed source. Therefore, engineering of nanocrystalline metals must be addressed differently from traditional materials.

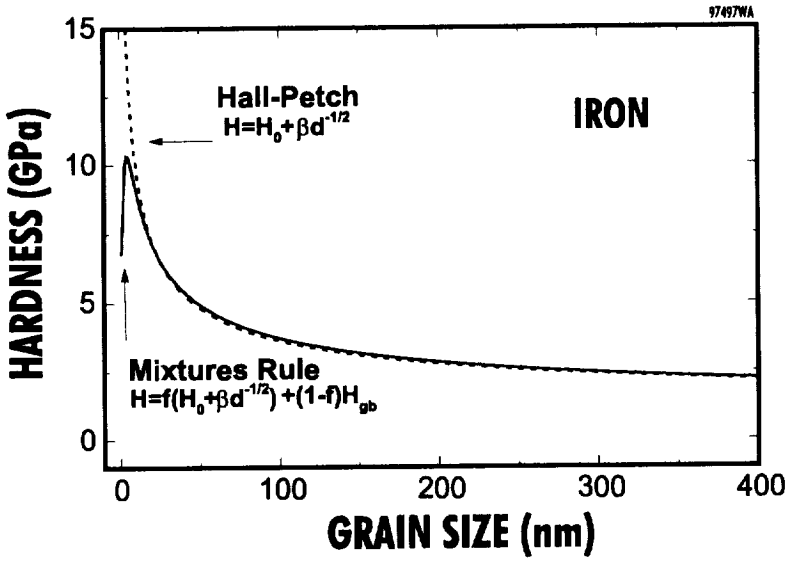

Figure 6 Relationship between hardness and grain size for iron, based on the Hall-Petch[3,4] relations and the mixture rule.[5]

2 PHASE I RESULTS

In Phase I, many homometallic stainless steel coated samples were produced and examined. Several important conclusions were drawn from this study. First, in comparison to uncoated 316 stainless steel, all of the coated samples were significantly harder. The uncoated stainless steel had a hardness of 4 GPa, while the hardest coated sample had a hardness of 13.3 GPa. Second, the coated samples also exhibited much less wear. The best of the coated samples had a wear rate *33 times* lower than the uncoated sample. There was *no* evidence of coating fracture or delamination in any of the coated samples. This indicates that adhesion was excellent.

All coatings deposited in Phase I exhibited hardness at least 200% higher than that of the bulk materials. Our measurements indicate that there is a direct relationship between nanohardness and the current density of the ion beam. Stress measurements indicate that film stress increases proportionally with current density of the ion beam. TEM, XPS, and XRD results indicate that the coated layers consist of FCC structure nanocrystallites with a dimension of about 10 to 100 nm. The Ni and Mo concentration of these coatings are lower than those of bulk 316L, but the concentration of Cr is higher.

2.1 Deposition of Nanocrystalline Homometallic 316L Stainless Coatings

After optimizing the IBAD process for deposition of 316 stainless steel, we carried out deposition of homometallic coatings under six different processing conditions. Substrates included 316L stainless steel coupons, Si wafers, and 0.005" thick spring steel stress coupons. As shown in Table 2, processing variations were limited to ion beam current density during coating and composition of the ion beam; initial coating runs were conducted with mixtures of Ar^+ and N_2^+ ions for a comparison with Ar^+ ions alone.

Coating thickness and stress were measured at Spire and are summarized in Table 2. Thickness was measured with a surface profilometer on flat coupons that were partially masked during deposition. Coating stress was measured from the curvature of spring steel coupons that were included in each run; positive values indicate compressive stress. Twelve stainless steel coupons coated with homometallic films and six coated Si substrates were sent to the University of New Hampshire, Spire's STTR partner in the program, for nanohardness measurements, wear testing, and analytical studies.

Table 2 Summary of homometallic stainless steel coating depositions.

Run number	Deposition rate (Å/sec)	Current density (uA/cm^2)	Ion beam energy (eV)	Ion beam gas	Thickness (micron)	Stress (ksi)
202040501	6	100	500	N / Ar (6 / 1)	1.56	19
202041003	6	100	500	N / Ar (1 / 1)	1.58	7
202041202	6	100	500	Ar	1.26	84
202041707	6	150	500	Ar	0.75	150
202041708	6	50	500	Ar	1.4	-71
202041709	6	100	300	Ar	1.22	63

2.2 Nanohardness Testing

Coating and substrate nanohardness was measured by nanoindentation with a Hysitron nano-mechanical test instrument equipped with a Berkovich indenter. Films were tested under a multiple loading sequence with loads up to 6 mN. Analysis of the resulting load-depth curves was carried out using the Oliver-Pharr method,[6] which yields both nanohardness and Young's modulus as a function of indenter depth. For each film, approximately 3-5 indents were made, with each of the multiple load sequences giving at least 10 hardness and elastic modulus values. Table 3 is a summary of nanohardness data for the homometallic stainless steel samples.

Table 3 Summary of nano-indentation data for homometallic stainless steel samples

Sample	Avg. Hardness (GPa)	Std. Dev.	Avg. Modulus (GPa)	Std. Dev.	H/E Ratio
Substrate	4.4	0.25	232.5	21	0.019
0501	9.6	0.7	172.4	5.4	0.056
1003	11.2	0.1	195.0	5	0.057
1202	8.2	1.1	171.7	13	0.048
1707	13.3	0.2	201.1	6.6	0.066
1708	5.6	1.6	116.2	33.2	0.048
1709	11	0.5	189.2	6.9	0.058

Figures 7 and 8 show hardness and elastic modulus measurements vs. depth for the substrate and coated samples, where each plotted point is an average of 5 indentations. Generally, the hardness varied little with depth, except for #1202, which gave somewhat different results. Overall, the data show a substantially higher hardness for the homometallic films compared to that of the substrate. The substrate had the lowest hardness (4.4 GPa) while sample #1707 had the highest (13 GPa). Elastic modulus values range from 170 to 250 GPa, with the modulus for the substrate material within the range of the films when tested at the same indentation depth. The fact that the hardness values for the films are higher, while the elastic modulus remains relatively constant, indicates that there is a true metallurgical strengthening mechanism operating in the deposited films.

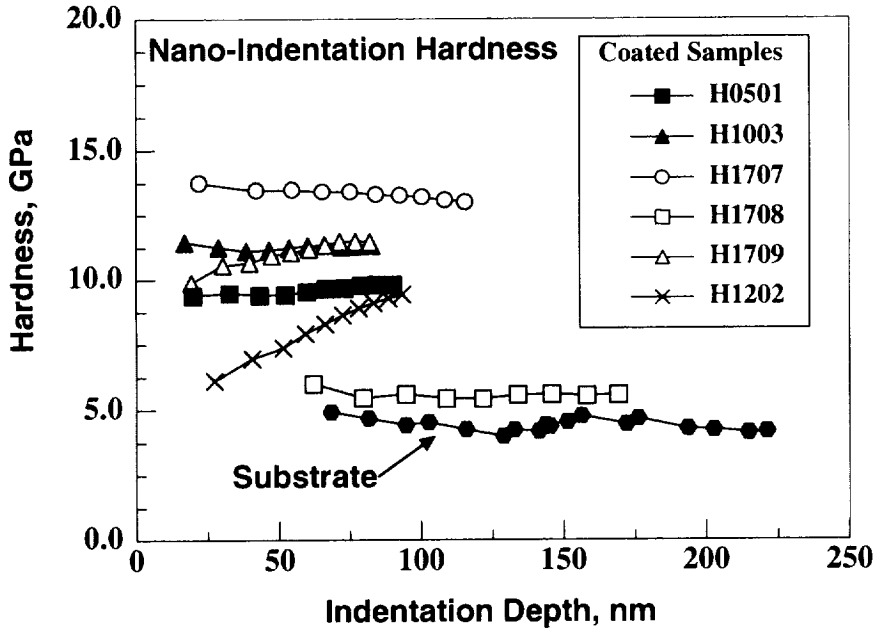

Figure 7 Hardness data for coated samples and the substrate. Data are shown as hardness vs. the indentation depth. Sample #1707 had the highest nanohardness, and the substrate material the lowest.

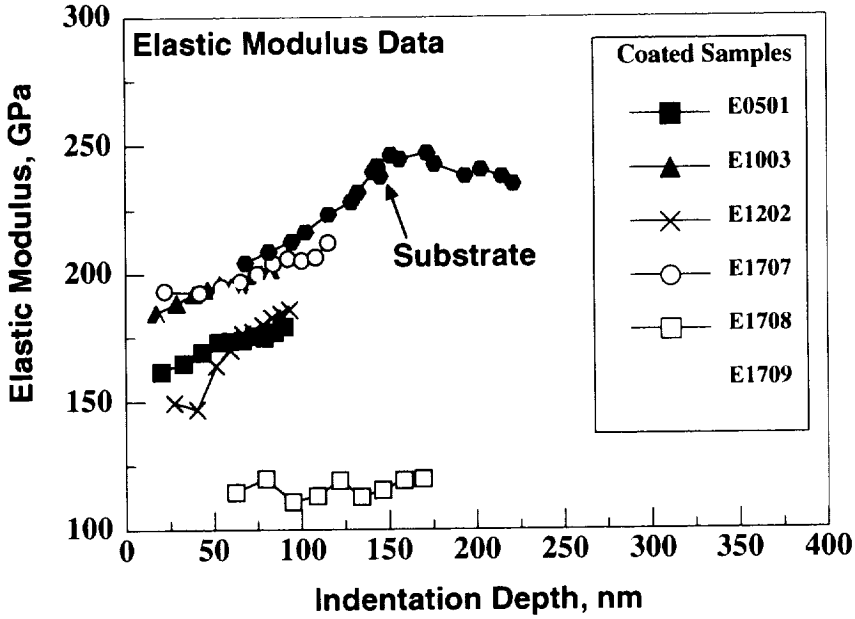

Figure 8 Elastic modulus data for coated samples and substrate material. Note the modulus of the substrate is not significantly different from that of the coatings.

An example of indentation curves is shown in Figure 9. Here we compare sample #1707 (under multiple loading) with the substrate material (single load curve). The film clearly shows higher hardness and lower indentation depth for the same maximum load.

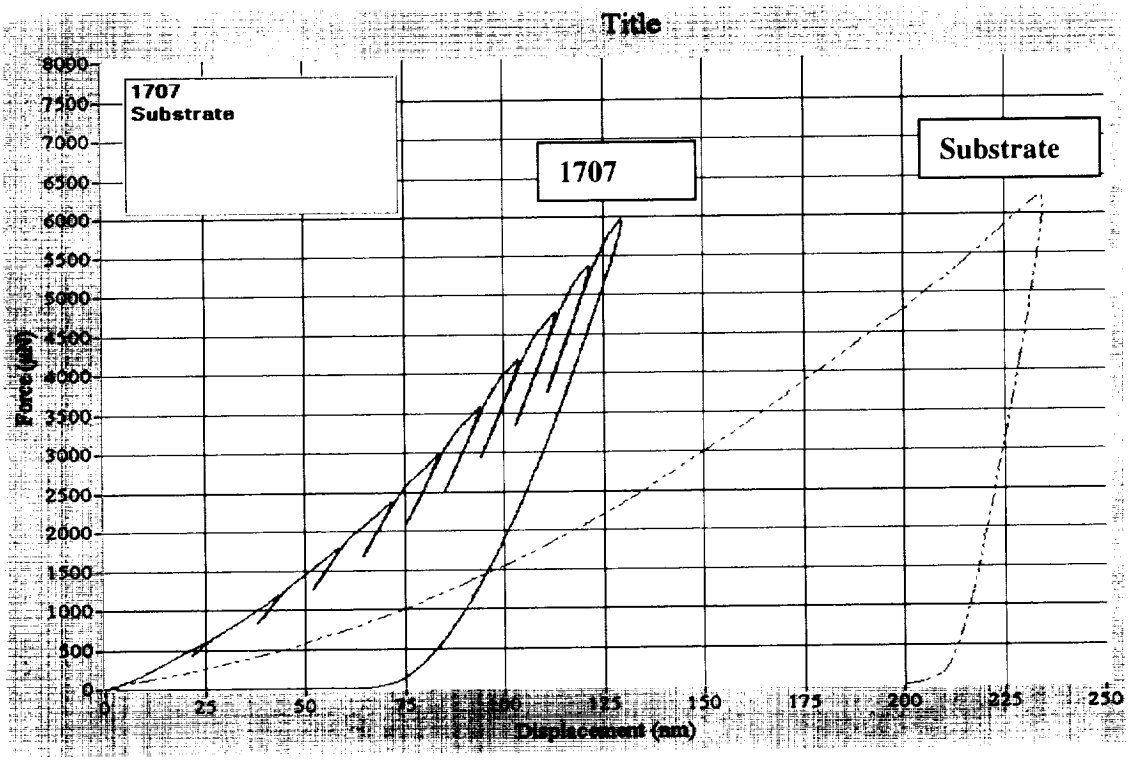

Figure 9 Examples of load-displacement curves for nano-indentation measurements.

2.3 Wear Resistance Measurements

Wear testing was performed on a pin-on-disk system that was designed and built in the Materials Laboratory of the University of New Hampshire. It features variable rotation speed, variable loads, and a computerized control and data acquisition system. Pin-on-disk wear tests were carried out on all samples. Conditions for the wear tests are given below:

Wear test procedure:
Type: Pin-on-disk
Ball Material: 316 Stainless Steel
Ball Size: ¼ in. diameter
Load: 132 gf
Contact Stress: 618 MPa
Rotation speed: 180 rpm
Atmosphere: Air
Temperature: Ambient
Lubrication: Light machine oil

The samples were run for a total of 1800 revolutions. During the test, the friction coefficient was measured. After that time, the test was terminated and the samples were cleaned and examined by optical microscopy. The widths of the wear tracks were measured in the optical microscope.

Friction coefficients were not significantly different for all tested samples and were in the range of 0.05 to 0.1 for the duration of the test. To obtain accurate information on wear, the wear tracks on the coupon disks were examined with a Tencor Alpha-Step profilometer. Depth versus. distance across the wear track was measured for each sample, and the area of wear below the sample surface was estimated from these traces. Wear volume was calculated by multiplying this area by the length of the wear track. Figure 10 shows example profilometer traces for uncoated and homometallic coated samples. The vertical scale is indicated for each trace. The results in Table 4 were generated from these data, which includes hardness data and measurements of the wear track width, obtained by optical microscopy.

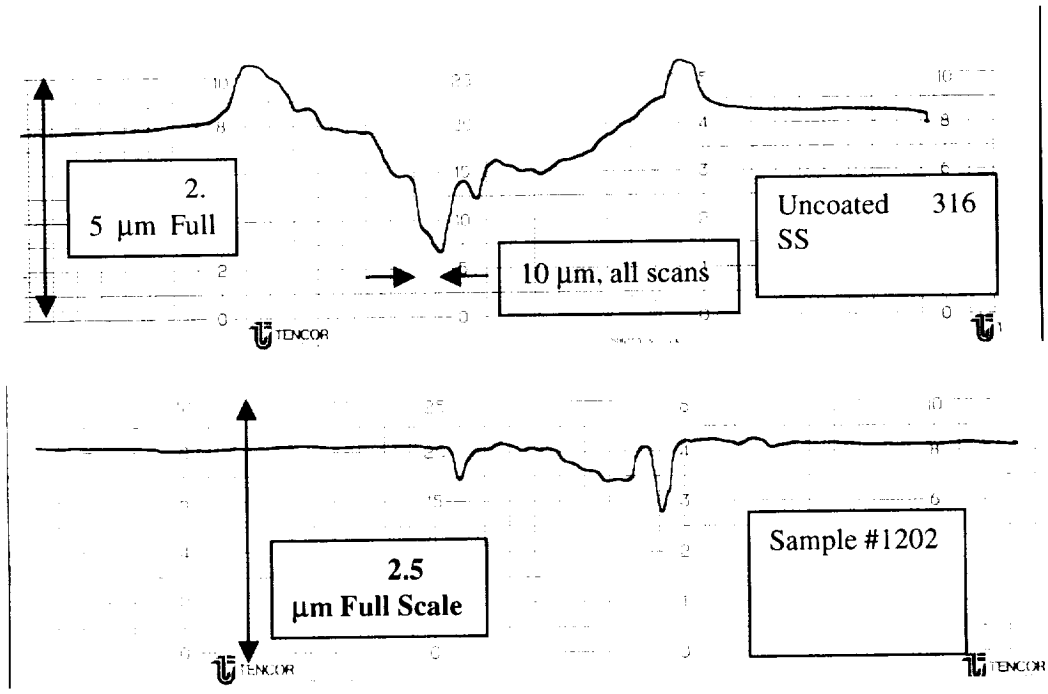

Figure 10 Representative profilometer traces of wear track for uncoated and coated samples.

The data of Table 4 show that all coated samples had less wear than the uncoated stainless steel sample. The samples that performed best according to the wear volume are #0501, 1707, 1202 and 1708. Samples 1003 and 1709 were significantly worse, even though they had among the highest hardness values. However, the sample with the lowest hardness, the uncoated control, exhibited the highest wear rate, by a factor of approximately 27. This indicates that correlations between wear and hardness are not simple, and that other factors beside hardness play a role in determining wear rates.

Table 4 Tribological and mechanical properties of substrate and coated samples.

Sample #	Wear Rate Volume/Rev (cm^3/cycle)	Depth of track μm (Profilometer Measurement)	Width of track μm (Optical Measurements)	Hardness GPa (Nano-indentation)
Uncoated 316 Stainless	$4.72x10^{-9}$	1.5	183	4.4
1708	$1.74x10^{-10}$	0.1	100	5.6
1202	$1.74x10^{-10}$	0.5	155	8.2
0501	$1.74x10^{-10}$	0.15	93	9.6
1709	$2.61x10^{-9}$	1.0	150	11
1003	$6.11x10^{-10}$	0.5	148	11.2
1707	$1.44x10^{-10}$	1.4	131	13.3

2.4 Analytical Studies

2.4.1 TEM and X-ray Diffraction Analysis

Four of the six samples, from runs of 1003, 0501, 1707 and 1202, were analyzed by transmission electron microscopy (TEM). The samples were prepared by mechanically dimpling on a VCR, Inc., D500 instrument, followed by ion milling on a Fishione, Inc. LAMP 1010 ion mill. The ion milling parameters were 3.5kV and 5.0 mA and a milling angle of 15°. Samples were examined in the plan-view orientation. After the samples were prepared, there were examined in a JEOL 2000FX TEM operating at 200 kV. These samples were examined in bright-field and dark-field imaging modes and also using electron diffraction. Bright-field image for sample 1003 shows a polycrystalline grain structure with a grain size of 10-20 nm. Electron diffraction pattern shows continuous rings confirms the presence of an ultra-fine grain structure. In this sample, there is a relatively low defect density within the grains, although there are some voids along the grain boundaries. TEM results for sample 0501 show an ultra-fine grain structure, on the order of 10-20 nm, although high magnification images show a much higher defect density (such as dislocations and nano-twins,) within the grains. The structure is also denser, and grain boundary voids are not observed.

Hardness data were 11.2 GPa for sample 1003 and 9.6 GPa for sample 0501. These values are very close, indicating that the grain size is largely responsible for the hardness levels observed, and that the presence of voids or defects did not have a major effect on the hardness in these samples.

Results of electron diffraction analysis are shown in Table 5 for sample #1003. The table also shows a comparison with X-ray diffraction data for the same sample. In general, the accuracy of d-spacing measurements by X-ray diffraction is not as good as for electron diffraction, and intensities of peaks can only be qualitatively estimated. In addition, the sample examined is in thin-film form, and preferred orientation in the film may cause certain peaks to be absent. However, measured lines for both methods are reasonably consistent. In addition, a set of lines corresponding to an FCC structure is observed, as indicated in the last column listing (hkl) planes. Some additional lines are present, indicating the possible formation of intermetallic compounds that have not yet been identified. Analysis of sample #0501 was also carried out. In general, peaks were more diffuse, but otherwise similar to those of sample #1003.

Table 5 Diffraction data for sample #1003: comparison of electron and x-ray diffraction results

vs = very strong; m = medium; w = weak; vw = very weak

TEM/Electron Diffraction		X-ray Diffraction		
d_{hkl}, nm	Intensity, rel	d_{hkl}, nm	Intensity, %	(hkl) for FCC
		0.233	6	
0.215	vs	0.216	8.7	
		0.210	100	(111)
0.191	m	0.191	2.9	(200)
		0.181	2.2	
0.173	w	0.175	7.1	
0.148	vw	0.136	38	(113)
0.128	vw	0.125	2.8	(220)
0.122	w	0.120	4.2	(222)

Summary: sample #1003 had a very small grain size, but also had numerous voids along the grain boundaries. These voids may be the reason for its relatively poor wear resistance. Sample 0501 had a very fine grain size, on the order of 10 nm, and exhibited excellent wear resistance along with a high hardness. The other two samples, 1707 and 1202 had relatively large grain sizes (~50-100 nm) but also exhibited good wear resistance and high hardness.

2.4.2 X-ray Photoelectron Spectroscopy (XPS)

The two samples (#1003 and 0501) examined by TEM were also analyzed by XPS with a Kratos Axis/HS system. MgKα X-radiation was employed, and spectra were collected with a pass energy of 160 eV, a step size of 0.5 eV, an energy range of 1100 to 0 eV, and sweep time of 120 seconds. Quantitative analysis was conducted using the software and standards supplied with the Kratos system.

Table 6 shows results of the quantitative compositional analysis, along with the nominal composition of type 316 stainless steel. The deposited films had a higher Cr concentration, and a lower Ni concentration in comparison to standard type 316 stainless steel. This may be due to unequal rates of evaporation of these elements during e-beam evaporation. No carbon, nitrogen or oxygen was detected by XPS.

2.4.3 Secondary Ion Mass Spectroscopy (SIMS) Analysis

Figures 11 and 12 show SIMS depth profiles of homometallic nanocrystalline 316L stainless steel coatings produced by IBAD (See Table 2 for deposition conditions). Compared to the substrate, the coated layer differs by approximately 10 to 20 percent in metals concentration, although this difference has no significant effect on mechanical properties of the coatings. Significant carbon and oxygen contamination is present at the interface between the coating and substrate. These interfacial impurities could reduce adhesion strength of the coating. Phase II work will develop processes to better clean substrate surfaces prior to coating.

Table 6 **Comparison of XPS, TEM, wear resistance measurements and nanohardness results. Compositions of coated samples are also compared with nominal composition of 316L stainless steel.**

Sample	Fe, wt.%	Cr, wt. %	Ni, wt. %	Mo, wt. %	N (O) ratio to Sub	Nano Hardness GPa	Wear Rate Volume/Rev (cm^3/cycle)	Crystal structures
316 SS, Nom.	Bal.	17	12	2.5	1	4.4	$4.72x10^{-9}$	
#0501 more N	75.7	21.6	2.3	0.5	47 (x)	9.6	$1.74x10^{-10}$	High defect density (such as dislocations and nano-twins) within the grains. denser structure, no grain boundary voids
#1003 less N	72.3	22.7	4.5	0.5	17 (x)	11.2	$6.11x10^{-10}$	low defect density, voids along the grain boundaries

n.d. = not detected

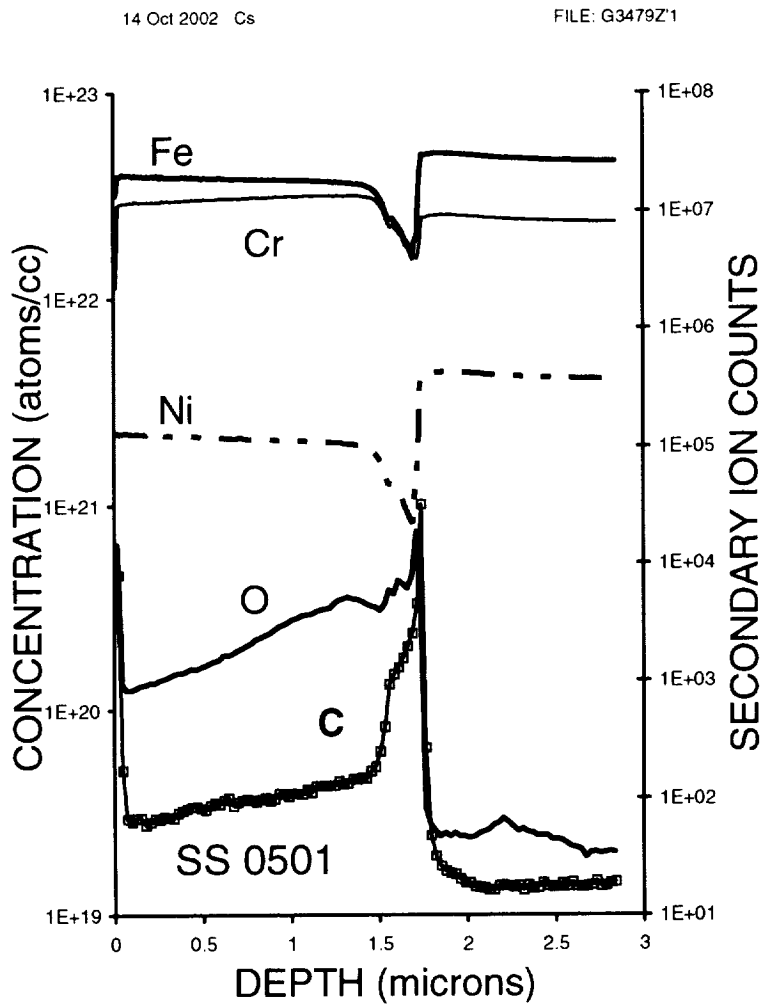

Figure 11 **SIMS depth profile of homometallic nanocrystalline coating run #0501. The presence of carbon and oxygen is accompanied by depletion of metals at the interface between coating and substrate.**

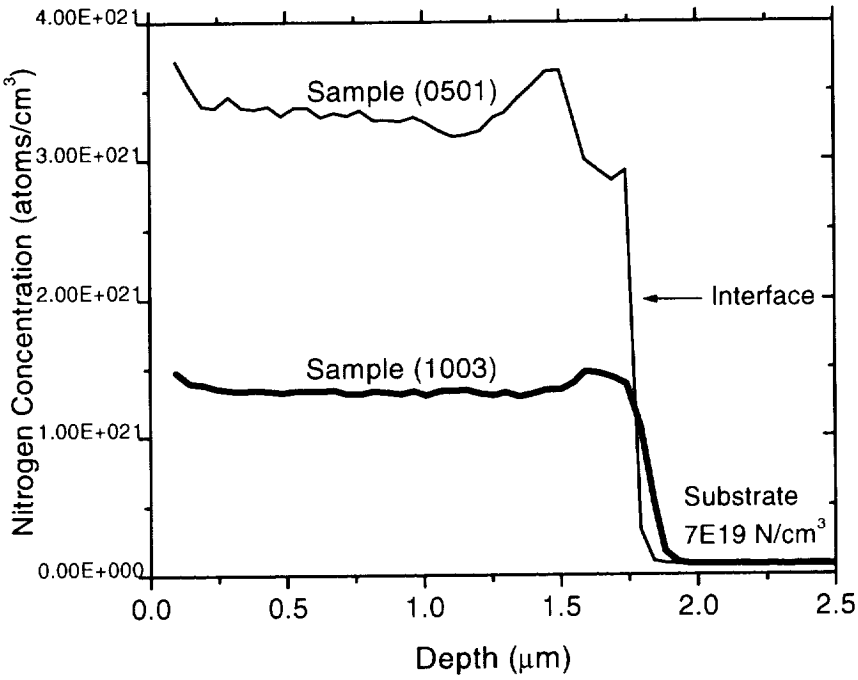

Figure 12 SIMS depth profiles comparing nitrogen concentration in homometallic nanocrystalline coatings of runs #0501 and #1003 (See Table 2 for deposition conditions). Relative amounts of oxygen were proportional to nitrogen concentration in the film.

2.5 Discussion - Dependence of Nanohardness on Process Conditions

Figures 13 through 16 and Tables 7 and 8 summarize nanohardness, stress, and thickness of nanocrystalline homometallic stainless coatings as a function of ion beam energies and current densities for a deposition rate of 6 A/sec. Figure 13 shows nanohardness *vs.* ion beam current density at 500 eV, indicating that higher hardness were obtained at higher beam densities. Figure 14 demonstrates higher stress in the film produced at higher ion beam densities. Figure 15 shows thickness of the coatings versus Ar beam current density; indicating a higher sputtering rate for higher ion beam current densities. Figure 16 demonstrates stress versus ion beam energy indicating higher stress for higher ion energies.

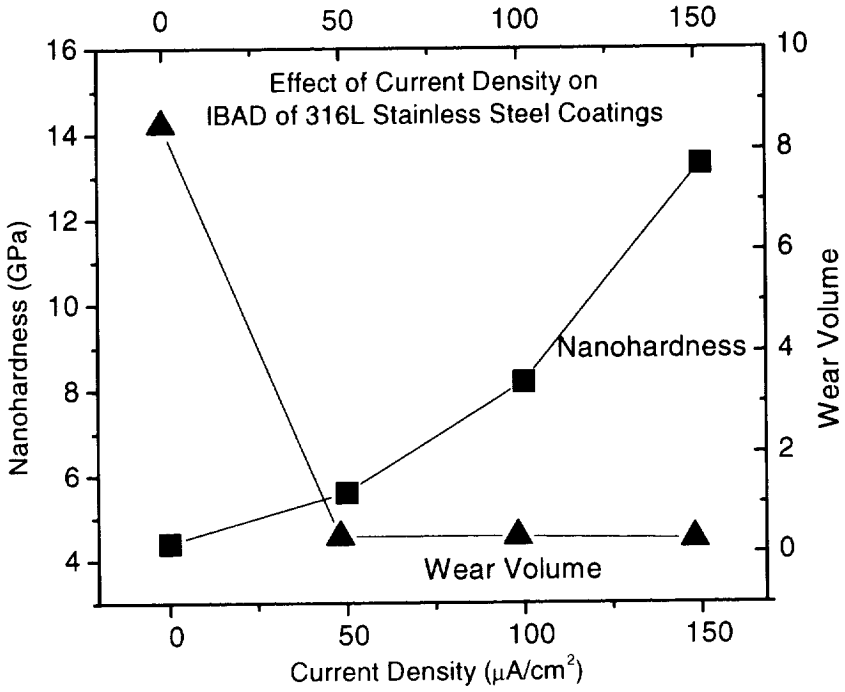

Figure 13 Nanohardness and wear volume versus ion beam current density at 500 eV for a deposition rate of 6A/sec, indicating that higher hardness can be obtained for higher beam densities. Note for the sake of comparison, bulk materials are represented by zero current density.

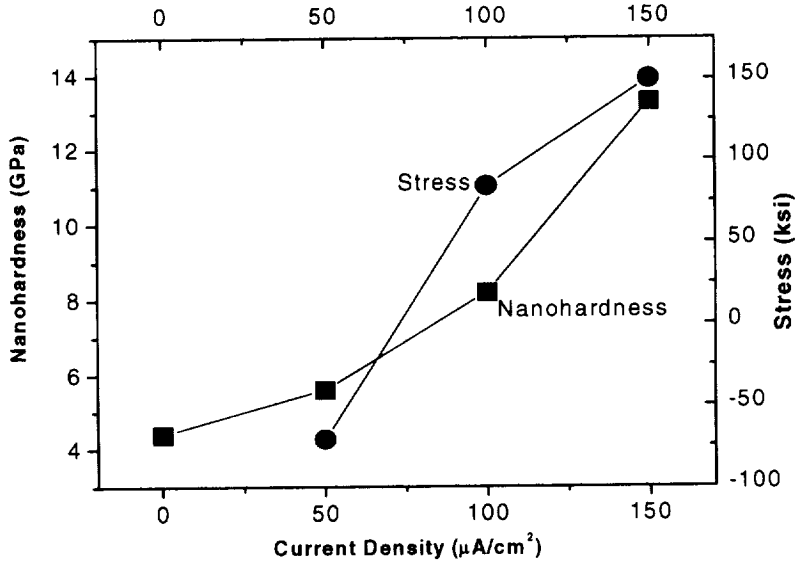

Figure 14 Coating stress versus ion beam current density at 500 eV for a deposition rate of 6 A/sec, indicating higher stress in the film for higher ion beam densities. Note that for the sake of comparison, bulk materials are represented by zero current density.

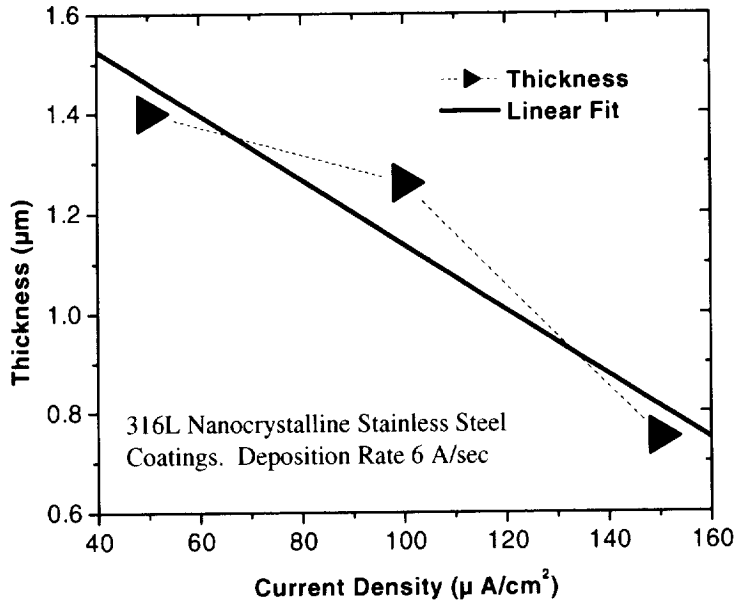

Figure 15 Thickness of the coatings versus Ar beam current density at 500 eV for a deposition rate of 6A/sec, indicating thinner films (higher sputtering rate) for higher ion beam currents.

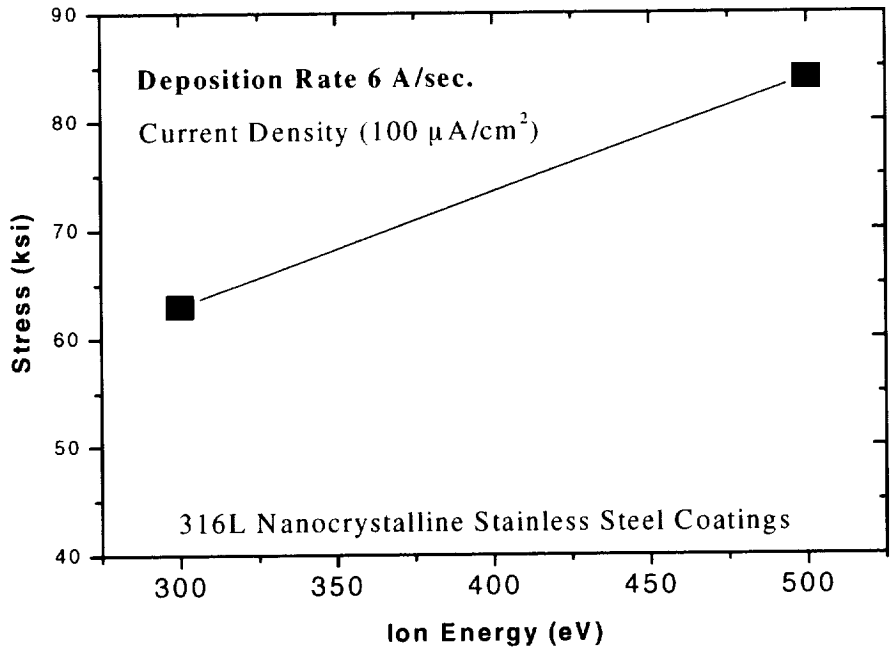

Figure 16 Coating stress versus ion beam energy at a deposition rate of 100 μA/cm², indicating higher stress for higher Ar ion beam energies.

Table 7 **Effect of argon ion beam energy on nanohardness, volume wear, thickness and film stress for a deposition rate of 6 Å/sec and ion current density of 100 μA/cm^2 at 500 eV.**

Run number	Deposition rate (Å/sec)	Current density (uA/cm^2)	Ion beam energy (eV)	Ion beam gas	Thickness (micron)	Stress (ksi)	Hardness, GPa (Nano-indentation)	Wear Rate Volume/Rev (cm^3/cycle)
Uncoated			0				4.4	4.72×10^{-9}
202041709	6	100	300	Ar	1.22	63	11	2.61×10^{-9}
202041202	6	100	500	Ar	1.26	84	8.2	1.74×10^{-10}

Table 8 **Effect of ion beam current density on nanohardness, volume wear, thickness and film stress For a deposition rate of 6 Å/sec and ion energy of 500 eV.**

Run number	Deposition rate (Å/sec)	Current density (μA/cm^2)	Ion beam energy (eV)	Ion beam gas	Thickness (μm)	Depth of track (μm)	Stress (ksi)	Hardness, GPa (Nano-indentation)	Wear Rate Volume/Rev (cm^3/cycle)
Uncoated								4.4	4.72×10^{-9}
202041708	6	50	500	Ar	1.4	0.1	-71	5.6	1.74×10^{-10}
202041202	6	100	500	Ar	1.26	0.5	84	8.2	1.74×10^{-10}
202041707	6	150	500	Ar	0.75	1.4	150	13.3	1.44×10^{-10}

2.6 Conclusions Of Phase I Research

We have formed nanocrystalline homometallic stainless steel coatings on 316L substrates by ion beam assisted deposition. We have studied the coatings for nanohardness, wear resistance, crystalline structure, film stress, and composition. For all deposition conditions we have produced smooth, uniform, superhard coatings. Although further analysis in Phase II is necessary, the following conclusions can be drawn:

1 Nanohardness of homometallic, nanocrystalline coated samples is at least 200% greater than that of the substrate (with a larger grains) materials. Samples produced at higher current density ion bombardment show an increase up to 400 percent.

2 Stress in the films increases proportionally with current density of ion beam. At very low current we measured tensile stress, while at high current densities we observed compressive stress.

3 All coated samples had reduced wear in comparison to uncoated 316 stainless steel (with the larger grain size). The wear volume on all coated samples was reduced in comparison to uncoated type 316 stainless steel. The best sample exhibited a factor of 27x lower wear rate than the uncoated sample.

4 XPS analysis of all coated samples had a higher Cr concentration, but lower Ni and Mo concentrations, in comparison to the composition of bulk 316 stainless steel.

5 SIMS depth profiling of two samples showed a higher Cr concentration, but lower Fe, Ni and Mo concentrations, in comparison to bulk 316 stainless steel. Furthermore, SIMS data clearly indicates significant concentrations of oxygen and carbon impurities at the interface between the coating and substrate material.

6 TEM analysis of two samples which were produced by Ar and (small amount of) N beams revealed a nano-crystalline grain structure with grain sizes on the order of 10-20 nm. Electron diffraction showed the structure was predominantly FCC.

7 TEM analysis of two samples which were produced by Ar-only beams revealed nano-crystalline sizes on the order 50-100 nm diameter grains. Electron diffraction showed the structure was predominantly FCC.

3 REFERENCES

1. J. K *Scientific American* (October 1996).
2. Holleck, *J. Vac. Sci. Technol.* A **4**, 2661 (1986).
3. O. Hall, *Proc. Phys. Soc. B* **64**, 747 (1951).
4. N.J. Petch, *J. Iron Steel Inst.* **174**, 25 (1953).
5. J.E. Carsley, J. Ning, W.W. Milligan, S.A. Hackney, and E.C. Aifantis, Nano-Structured.
6. W.C. Oliver and G.M. Pharr, J. Mater. Res. 7, 1564 (1992).

CLASSIFIED BY:

DECLASSIFY ON:

	Form Approved OMB No. 0704-0188

1. AGENCY USE ONLY *(Leave blank)*	2. REPORT DATE	3. REPORT TYPE AND DATES COVERED
	12/19/2002	Final Report

4. TITLE AND SUBTITLE	5. FUNDING NUMBERS
Superhard Nanocrystalline Homometallic Stainless Steel on Steel for Seamless Coatings	NAS1-02041
6. AUTHOR(S) Eric J. Tobin	
7. PERFORMING ORGANIZATION NAME(S) AND ADDRESS(ES) Spire Corporation One Patriots Park Bedford, MA 01730	8. PERFORMING ORGANIZATION REPORT NUMBER 60436
9. SPONSORING/MONITORING AGENCY NAME(S) AND ADDRESS(ES NASA/Langley Research Center 9A Langley Boulevard Hampton, VA 23681-2199	10. SPONSORING/MONITORING AGENCY REPORT NUMBER
11. SUPPLEMENTARY NOTES	
12a. DISTRIBUTION/AVAILABILITY STATEMENT	12b. DISTRIBUTION CODE

13. ABSTRACT (*Maximum 200 words*)

The objective of this work is to deposit nanocrystalline stainless steel onto steel substrates (homometallic) for enhanced wear and corrosion resistance. Homometallic coatings provide superior adhesion, and it has been shown that ultrafine-grained materials exhibit the increased hardness and decreased permeability desired for protective coatings. Nanocrystals will be produced by controlling nucleation and growth and use of an ion beam during deposition by e-beam evaporation or sputtering.

Phase I is depositing 316L nanocrystalline stainless steel onto 316L stainless steel substrates. These coatings exhibit hardnesses comparable to those normally obtained for ceramic coatings such ZrO2, and possess the superior adhesion of seamless, homometallic coatings. Hardening the surface with a similar material also enhances adhesion, by avoiding problems associated with thermal and lattice mismatch

So far we have deposited nanocrystalline homometallic 316L stainless steel coatings by varying the ions and the current density of the ion beams. For all deposition conditions we have produced smooth, uniform, superhard coatings.

All coatings exhibit hardness of at least 200% harder than that of bulk materials. Our measurements indicate that there is a direct relationship between nanohardness and the current density of the ion beam. Stress measurements indicate that stress in the films is increasingly proportional to current density of the ion beam. TEM, XPS, and XRD results indicate that the coated layers consist of FCC structure nanocrystallites with a dimension of about 10 to 20 nm. The Ni and Mo concentration of these coating are lower than those of bulk 316L but the concentration of Cr is higher.

14. SUBJECT TERMS	15. NUMBER OF PAGES
Super hard, Nanocrystalline, Stainless Steel, seamless, coatings, adhesion, ion beam, corrosion	22
	16. PRICE CODE

17. SECURITY CLASSIFICATION OF REPORT	18. SECURITY CLASSIFICATION OF THIS PAGE	19. SECURITY CLASSIFICATION OF ABSTRACT	20. LIMITATION OF ABSTRACT
Unclassified	Unclassified	Unclassified	Unclassified

nsn 7540-01-280-5500

Standard Form 298 (Rev. 2-89)
Prescribed by ANSI Sts 239-18